Geometry dependence of nonlinear effects in high temperature superconducting transmission lines at microwave frequencies

James C. Booth,[a] J. A. Beall, D. A. Rudman, L. R. Vale, and R. H. Ono
National Institute of Standards and Technology, Boulder, Colorado 80303

(Received 18 January 1999; accepted for publication 12 April 1999)

We investigate the nature of low-power nonlinear effects in high-temperature superconducting microwave devices by measuring third harmonic generation at 76 K in coplanar waveguide transmission lines of different geometries fabricated from $YBa_2Cu_3O_{7-\delta}$ thin films. The measured power in the third-harmonic signal changes systematically with film thickness, center conductor linewidth, and line length. We analyze these results using a simple model for a transmission line with a nonlinear inductance arising from a current-dependent superconducting penetration depth. This analysis describes quantitatively the observed differences in harmonic generation for transmission lines of different dimensions, and yields a single geometry-independent parameter (the nonlinear scaling current density J_0) to quantify the observed nonlinear behavior. For the thin film samples studied here $J_0 = 3.0 \times 10^7$ A/cm^2 at 76 K for all geometries investigated. These results provide the means to establish a lower limit for the expected nonlinear response of superconducting components of arbitrary geometry at microwave frequencies. [S0021-8979(99)05614-5]

I. INTRODUCTION

High temperature superconductors are finding increasing application in passive microwave elements such as filters and delay lines, which benefit from the extremely low surface resistance and relatively high transition temperature ($T_c \sim 90$ K) characteristic of these materials.[1,2] The advantage of high temperature superconductor (HTS) devices can be compromised, however, by factors such as the rapid increase in loss at high microwave powers[3,4] and nonlinear effects generated at all powers.[5] An example of the potentially serious problems due to nonlinearity is intermodulation distortion in HTS transmit/receive filters, where two signals within the passband of a filter are mixed by nonlinear processes to produce interference signals which can also fall within the passband.[1] It is not known if such nonlinear effects in HTS devices are an inherent property of HTS materials or occur as a result of the device fabrication process. The achievable limits on device linearity are therefore impossible to predict.

To better understand the nature of nonlinear effects in HTS microwave devices, we investigate the role of device geometry on the nonlinear response of HTS coplanar waveguide (CPW) transmission lines. The goal of these experiments is to determine whether the observed nonlinear effects in HTS devices are of intrinsic or extrinsic origin, and to facilitate the comparison of nonlinear measurements obtained for structures of different geometries. The results of these experiments can then be used to help develop thin film and device fabrication processes which minimize nonlinear effects in HTS microwave devices, and to predict the level of nonlinear response in actual HTS applications.

Many HTS microwave applications are implemented using thin films in planar geometries, such as microstrip, strip line, and coplanar waveguide.[6] While allowing for substantial reduction in component size and weight, planar devices usually carry larger current densities than three-dimensional structures, which increases nonlinear effects. Nonlinear behavior is typically observed as intermodulation distortion (IMD) in filters and resonators[7–10] and as harmonic generation in broadband devices such as transmission lines.[5,11] Higher harmonics and intermodulation products are two different manifestations of the same nonlinear processes, and they can be simply related.[1,12] Even so, it is currently difficult or impossible to compare the measured nonlinear response in different structures owing to differences in device geometry (e.g., microstrip, strip line, coplanar waveguide) and device dimensions (film thickness, conductor length, width). Different experimental configurations can give nonlinear responses that differ by orders of magnitude for similar input powers, yielding little information about the sources of the observed nonlinear behavior.

In this article we present measurements of nonlinear effects in CPW transmission lines of different geometries which are fabricated from HTS thin films. We expand on previous work[13] to directly compare the results of these measurements with the predictions of a simple model. To quantify the nonlinear response of our HTS microwave devices, we measure third harmonic generation as a function of incident power.[5] We use single frequency third harmonic measurements and simple linear geometries in an effort to extract the underlying nonlinear material properties. In addition, we restrict our attention to microwave powers that correspond to current densities well below the critical current density of the superconductor in order to avoid the high power region where the surface impedance begins to rapidly increase with increasing power.[3,4]

The model that we use, developed by Dahm and Scalapino,[14] assumes the existence of a nonlinear inductance

[a]Electronic mail: booth@boulder.nist.gov

arising from a current-dependent penetration depth. A current-dependent penetration depth can arise from a number of sources, including current-induced depairing of the superconducting charge carriers, or from the presence of weak links.[14,15] Vortex motion has also been suggested as a source for a nonlinear reactance.[16] We adapt the model of Dahm and Scalapino, which calculates the intermodulation products in a microstrip resonator, to the case of third harmonic generation in planar transmission lines of variable length. Comparisons between the model and experimental results are accomplished by extracting the third-order intercept (described in detail below), which is defined as the incident power at which the measured third harmonic response would become equal in magnitude to the fundamental signal. By comparing the third-harmonic generation of CPW transmission lines of different dimensions, we are able to demonstrate that the nonlinear response of these devices changes with geometry exactly as predicted by the simple model. As a result, we can extract a single parameter (the nonlinear scaling current density J_0) to describe the observed nonlinear response of all of our devices, independent of specific geometry. These results suggest that the nonlinear response of our samples can be considered to be an intrinsic material property and is not generated by damage due to patterning, for example. The values obtained for the nonlinear scaling current density J_0 can then be combined with the theory of Dahm and Scalapino[14] to allow for the estimation of material limits on the smallest nonlinear effects achievable in practical superconducting microwave devices of arbitrary geometry.

II. THIRD-HARMONIC MEASUREMENTS

We fabricate CPW transmission lines from epitaxial *c*-axis-oriented $YBa_2Cu_3O_{7-\delta}$ (YBCO) films of different thicknesses grown by pulsed-laser deposition on 15 $\times$15 mm $LaAlO_3$ substrates. The films are grown at 770 °C (Ref. 17) at an oxygen pressure of 27 Pa (200 mTorr), with a thin ($\sim$20 nm) buffer layer of CeO_2 deposited between the YBCO film and the substrate. Prior to device patterning, the surface resistance (R_s) of the superconducting films is measured using a sapphire dielectric resonator operating at 17.5 GHz. The thickest films (500 nm) have a surface resistance at 76 K and 17.5 GHz of 735 $\mu\Omega$ (scaling by f^2 to 10 GHz gives $R_s = 240\,\mu\Omega$). In addition, the penetration depth λ is measured inductively at 76 K on representative samples[18] (these measurements yield $\lambda = 290$ nm at 76 K for the 500 nm thick samples). The films are patterned into CPW structures using standard optical photolithography and Ar ion milling. The CPW geometry is used in part because only one film is required (the center conductor and ground planes on either side are all located on the same surface of the film). In addition, the current density in the CPW geometry is peaked at the edges of the center conductor, making this configuration potentially very sensitive to processing damage at the conductor edges. More details of the unpatterned film properties and device fabrication can be found in Ref. 13.

To compare the nonlinear response of different device geometries, we fabricate up to 15 CPW transmission lines of different length and center conductor linewidth on the same

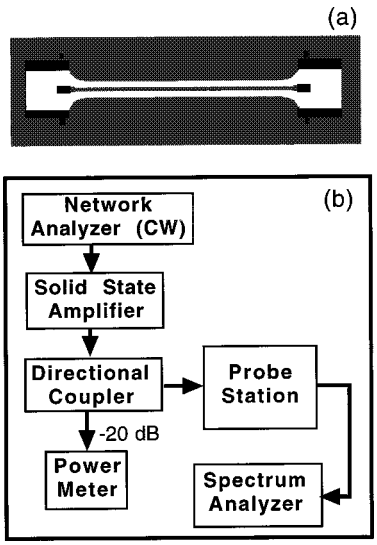

FIG. 1. (a) Diagram of a coplanar transmission line, showing use of tapers. The gray region is the YBCO, while the black rectangles are gold contacts. (b) Block diagram of the experimental setup to measure third harmonic generation in HTS transmission lines.

15$\times$15 mm YBCO chip. This helps ensure that the material quality for different transmission lines is nearly identical, so that the measured response reflects geometrical differences only. The gaps between the CPW center conductor and the ground planes on either side are adjusted to maintain 50 Ω characteristic impedance for the different center conductor linewidths. The individual transmission lines are characterized using a cryogenic microwave probe station, which uses air coplanar probes that are cooled under vacuum along with the sample, and which can be positioned *in situ* to make contact with the different CPW lines on the superconducting sample. Since the signal-to-ground separation of the coplanar contacts on the probes is fixed at 150 μm, exponential tapers are used onchip to transform to arbitrary center conductor and gap dimensions [see Fig. 1(a)]. The probe station allows measurement of all the devices on a given chip during a single cooldown, and sample temperatures down to 20 K are easily achieved. More details of probe station measurements of superconductors can be found in Refs. 13 and 19.

We measure third-harmonic generation to quantify the nonlinear response of our CPW devices. We use this technique, rather than intermodulation measurements, because our transmission lines are broadband devices, supporting the propagation of a fundamental signal at a frequency f and also the third harmonic signal at frequency $3f$. The harmonic generation method is relatively simple, requiring only a single input tone, and the power incident on the test devices can be determined without additional measurements of the input and output coupling. Nonresonant measurements also benefit from a simpler longitudinal current distribution (no standing wave patterns with adequate impedance matching), and are in general much less sensitive to the exact frequency of operation (no requirement for the signals to fall within a narrow passband). Another advantage is the fact that the

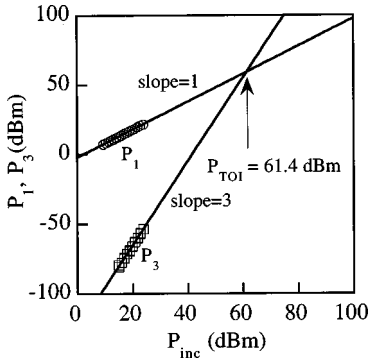

FIG. 2. Measured fundamental (5 GHz) and third harmonic (15 GHz) vs incident power at 76 K for a CPW transmission line fabricated from a YBCO thin film. The geometry of the transmission line is: linewidth $=21\ \mu$m, line length$=11.35$ mm, and film thickness$=320$ nm.

transmission line length can easily be varied at the frequency of operation.

Figure 1(b) shows a block diagram of the experimental configuration for our third-harmonic measurements. A vector network analyzer is used as a source in continuous wave (cw) mode to provide a single-frequency signal, which for these measurements is fixed at 5 GHz. This signal is fed into a solid state amplifier, which provides powers up to approximately 1 W, followed by a low-pass filter to remove higher harmonics generated by the source and amplifier. A directional coupler inserted in the signal path just before the probe station is used with a power meter to measure the power incident on the transmission line under test. After the signal passes through the probe station and the superconducting transmission line, the fundamental and any generated harmonics are measured using a spectrum analyzer. The measured return loss in this configuration when the amplifier is bypassed is typically greater than 20 dB, indicating adequate impedance matching to the CPW transmission lines.

The limit on the smallest harmonic signal generated by the superconducting transmission lines that can be detected depends on the sensitivity of the spectrum analyzer and the magnitude of any background harmonics generated by other components in the test setup. The measurement limit of the spectrum analyzer depends primarily on the resolution bandwidth, and also on factors such as input attenuation and averaging. For the measurements presented here, the spectrum analyzer sensitivity limit is approximately -84 dBm (the units of power quoted from this point forward are decibels referred to 1 mW, abbreviated dBm). In a configuration where the probe station is bypassed, no measurable background third-harmonic signal is detected up to an incident power of 28.3 dBm, the maximum power available for these measurements.

Figure 2 shows the measured power in the third harmonic and the fundamental as a function of incident power at 76 K for a 21 μm wide, 11.35-mm-long CPW transmission line fabricated from a 320-nm-thick YBCO film. The data in Fig. 2 show that the magnitude of the third harmonic rises with approximately slope 3 over the measured range of incident power. The measured power in the fundamental, in contrast, rises with a slope of 1 on the log-log plot, and has an

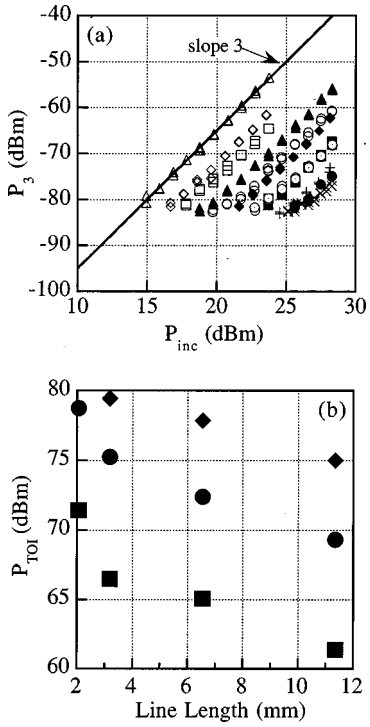

FIG. 3. (a) Measured third harmonic vs incident power at 76 K for eleven different CPW transmission lines of different geometries fabricated on a 320 nm YBCO thin film. Data are shown for the following lines: 21 μm wide, 2.06 mm long (open circles); 21 μm wide, 3.18 mm long (open squares); 21 μm wide, 6.54 mm long (open diamonds); 21 μm wide, 11.35 mm long (open triangles); 53 μm wide, 2.06 mm long (filled circles); 53 μm wide, 3.18 mm long (filled squares); 53 μm wide, 6.54 mm long (filled diamonds); 53 μm wide, 11.35 mm long (filled triangles); 105 μm wide, 3.18 mm long ($\times$); 105 μm wide, 6.54 mm long ($+$); 105 μm wide, 11.35 mm long (open circles with dots). (b) Resulting third order intercepts vs. transmission line length for the data shown in (a). The linewidths are 105 μm (diamonds), 53 μm (circles), and 21 μm (squares).

intercept close to 0. For the range of incident powers shown in Fig. 2, we estimate[1] the peak rf field strengths to be in the range from 2 to 6 mT (20–60 Oe).

We can quantify the nonlinear response shown in Fig. 2 by fitting the third harmonic data to a line of slope 3 and extracting the intercept point. By convention, we extract the third-order intercept point (P_{TOI}), which is the incident power at which a line of slope 3 fitted to the third-harmonic data intercepts a line of slope 1 fitted through the fundamental data.[20] The third-order intercept defined in this manner is not a realizable power; in practice the rf current densities exceed the critical current density of the superconductor well before the incident power approaches the third order intercept power. Figure 2 shows that a higher third-order intercept corresponds to a smaller third-harmonic signal for a given incident power; hence a higher third-order intercept implies a smaller nonlinear response for a given circuit.

Figure 3(a) shows the measured power in the third harmonic as a function of incident power for eleven transmission lines fabricated on a single YBCO chip. There are three sets of lines of width 21, 53, and 105 μm. The 21 and 105 μm linewidth structures use 0.2-mm-long exponential tapers to transform from a probe-compatible geometry (tapers are not required for the 53-μm-linewidth structures, which have

constant linewidth sections of corresponding lengths to the tapers). Within each of the constant linewidth sets are transmission lines of length 2.06, 3.18, 6.54, and 11.35 mm, for a total of twelve lines, each having a different geometry (these specified lengths include the 0.2-mm-transformer sections). We extract a third-order intercept (P_{TOI}) for eleven data sets in Fig. 3(a) and plot the resulting intercepts as a function of line length in Fig. 3(b) (each linewidth set is denoted by a different plotting symbol). The 2.06-mm-long transmission line of the 105-μm-linewidth set showed no measurable third-harmonic signal up to our maximum incident power. Figure 3(b) shows that decreasing the center conductor linewidth results in a lower P_{TOI} (implying a larger third-harmonic signal for a given incident power). This is qualitatively what we expect, since the smaller linewidth lines carry a larger current density for a given input power. Figure 3(b) also shows that P_{TOI} decreases with increasing line length for each set of lines.

The fact that the measured third-order intercept varies with the length and width of our superconducting transmission lines suggests that the observed third harmonic signal is generated predominantly by the transmission line itself, rather than by probes, contacts, tapers, or connectors (harmonic generation due to these factors would be constant and not change with transmission line geometry). For further verification, we have performed measurements on gold lines deposited on $LaAlO_3$ substrates (the gold lines have a linewidth of 53 μm and a gap spacing of 101 μm). Measurements of gold lines of different lengths at room temperature and at cryogenic temperatures (30 and 76 K) show no measurable third-harmonic signal for the maximum incident powers available for these experiments. These measurements of gold transmission lines also effectively exclude the $LaAlO_3$ substrate as a possible source of the observed nonlinear response.

III. CALCULATION OF THIRD HARMONIC GENERATION

To describe the observed nonlinear effects in our CPW devices, we calculate in this section the third harmonic generation due to the nonlinear inductance of a section of transmission line. We reproduce here the derivation of Dahm and Scalapino[14] to obtain an expression for the nonlinear contribution to the inductance due to a current-dependent penetration depth. However, instead of calculating the intermodulation power in a fixed length resonator as in Ref. 14, we calculate the third-harmonic generation in a variable length transmission line. In this treatment, we do not include the effects due to a nonlinear resistance, since we expect the effects of the nonlinear inductance to dominate the observed nonlinear response for superconducting transmission lines.

We follow Dahm and Scalapino[14] and define an expansion for the nonlinear inductance per unit length:

$$L(I)=L_0+L'I^2, \tag{1}$$

where L_0 is the linear (current-independent) contribution to the inductance, and L' is the nonlinear contribution, which is due to the variation of the penetration depth λ with the current density J. Because higher-order terms are neglected in Eq. (1), this expansion is valid only when the nonlinear response can be considered to be small. The expression for the nonlinear (current dependent) penetration depth is given by

$$\lambda^2(T,J)=\lambda^2(T)\left[1+\left(\frac{J}{J_0(T)}\right)^2\right]. \tag{2}$$

We label the parameter J_0 as the nonlinear scaling current density. Using the expression for the inductance per unit length:[14]

$$L=\frac{\mu_0\int(H^2+\lambda^2J^2)dS}{(\int J\,dS)^2}, \tag{3}$$

we obtain for the nonlinear contribution to the inductance

$$L'=\frac{\mu_0\lambda^2(T)\Gamma}{w^2t^2J_0^2}, \tag{4}$$

where Γ is a geometrical factor given by

$$\Gamma=\frac{w^2t^2\int J^4\,dS}{(\int J\,dS)^4}. \tag{5}$$

The integration in Eq. (5) is taken over the cross section of the transmission line conductor(s). In Eq. (5) it is important to use a form for the current density that is appropriate for the transmission line geometry under consideration, because J will in general be a strong function of position across the transmission line for many planar structures.

We now use the nonlinear inductance described by Eq. (1) to calculate third harmonic generation in a section of transmission line. Throughout the derivation we assume that the nonlinear term in the inductance generates a third harmonic signal, but does not appreciably affect the linear properties of the transmission line.

To determine the effect of the nonlinear inductance in Eq. (1) on the measured response of our circuit, we follow Ref. 21 and calculate the voltage generated by a (lumped element) nonlinear inductor of length l:

$$V(t)=lL(I)\frac{dI}{dt}=lL_0\frac{dI}{dt}+lL'I^2\frac{dI}{dt}. \tag{6}$$

For the time being, we assume that the inductor length l is small enough compared to a wavelength that a lumped-element approach is valid. We assume a single-tone input signal at an angular frequency ω:

$$I(t)=I_0\cos(\omega t). \tag{7}$$

Substituting Eq. (7) into Eq. (6) produces a voltage signal at frequency 3ω:

$$V(3\omega)=-\frac{lL'\omega I_0^3}{4}\sin(3\omega t). \tag{8}$$

We now calculate the power in the third harmonic for a section of transmission line of characteristic impedance Z_0:

$$P_3=\frac{1}{2Z_0}|V_3|^2=\left(\frac{\omega L'l}{4}\right)^2\frac{I_0^6}{2Z_0}=\left(\frac{\omega L'l}{2Z_0^2}\right)^2\frac{I_0^6Z_0^3}{8}. \tag{10}$$

Using the expression for the power in the fundamental $P_1=I_0^2Z_0/2$ we obtain

$$P_3(\mathrm{dB}) = 10\log_{10}(P_3) = 2\times 10\log_{10}\left(\frac{\omega L' l}{2Z_0^2}\right) + 3\times 10\log_{10}(P_1). \quad (11)$$

If we plot the power in the third harmonic versus the incident power (which is the same as the transmitted power in the fundamental for a lossless line), we obtain a line of slope 3 with an intercept given by the first term in Eq. (11). It is easy to show[20] that for a line of slope 3 with an intercept b, the third-order intercept is simply $P_{\mathrm{TOI}} = -b/2$. After substituting for L' in Eq. (11) we then obtain the following expression for the third-order intercept, in units of dBm:

$$P_{\mathrm{TOI}} = 10\log_{10}\left(\frac{2J_0^2(T)}{\mu_0\omega\lambda^2(T)}\frac{w^2t^2Z_0^2}{\Gamma l}\right) + 30. \quad (12)$$

The third-order intercept is found to depend on the dimensions of the transmission line, the characteristic impedance Z_0, as well as the material parameters λ and J_0.

There are some limitations to the application of the derivation of P_3 and P_{TOI} presented above. First, Eq. (1) must describe the current-dependent inductance with sufficient accuracy. For superconductors carrying large enough currents, the form of $L(I)$ is expected to deviate from that given in Eq. (1), and the analysis presented here will no longer be valid. For this situation, higher order terms in Eq. (1) will become important and must be considered. For this reason, we restrict our analysis to third harmonic data that increase with the third power of the incident signal, as illustrated in Fig. 2.

The second limitation is due to the fact that the expression in Eq. (12) was derived using a lumped-element approach for a nonlinear inductor, which can be strictly applied to transmission line sections where the length l is small compared to a wavelength. We can circumvent this difficulty to some extent by considering a general transmission line of length L as made up of a series of smaller transmission line elements such that the assumption $l \ll \lambda$ is valid for each segment. We then make the further assumption that the nonlinear responses from the individual segments do not interact and that the resulting third harmonic signals from each segment add in phase.[22] Obviously, this argument cannot be extended to arbitrarily long transmission lines because Eq. (10) would predict that P_3 will increase without bound as the length l increases, while P_1 remains constant. This apparant violation of conservation of energy results from the fact that in the current treatment we have ignored both the effects of losses and the effect of the nonlinear response on the fundamental signal. Therefore, the second practical limitation is that the third harmonic signal must remain much smaller than the fundamental signal. For the data that we present here, this condition $P_3 \ll P_1$ is always satisfied.

IV. DATA ANALYSIS

We can use the expression in Eq. (12) to compare our measured third-order intercept data for transmission lines of different geometries. In what follows, we will first demonstrate the application of Eq. (12) to describe differences in measured third-order intercepts for lines of different widths and lengths shown in Fig. 3 (b). We will then apply Eq. (12) to describe differences in the measured P_{TOI} for transmission lines fabricated from samples of different thickness. The use of Eq. (12) to scale our P_{TOI} measurements for different geometry transmission lines to the same reference geometry also enables us to extract an average P_{TOI} and a standard deviation for all transmission lines on a single chip regardless of the transmission line geometry. Finally we will use values for λ obtained from independent measurements to extract a value for the nonlinear scaling current density J_0 at 76 K for each film studied.

To illustrate the use of Eq. (12) to compare the third-order intercepts of transmission lines of different dimensions, consider two transmission lines that differ only in the center conductor width w. We can use Eq. (12) to calculate the expected difference in third-order intercept for these two lines. Assuming all other quantities are identical, we obtain

$$\Delta P_{\mathrm{TOI}}(\mathrm{dB}) = (P_{\mathrm{TOI}})^{\mathrm{line1}} - (P_{\mathrm{TOI}})^{\mathrm{line2}} = 20\log_{10}\left(\frac{w_s^{\mathrm{line1}}}{w_s^{\mathrm{line2}}}\right). \quad (13)$$

Consider, for example, transmission lines that differ in width by a factor of 5. From Eq. (13) we expect the third-order intercept of the narrower line to be lower by a factor of $20\log_{10}(5) = 14\,\mathrm{dB}$, which is roughly the difference we observe in Fig. 3(b) between the 21 and 105 μm lines. In practice the factor Γ in Eq. (12) will also change for different geometries, since the current distribution will be different for different linewidth samples. We use the method of Sheen[23] to calculate the current distributions for different transmission line dimensions, assuming a current-independent inductance. We then use Eq. (5) to determine the geometry factor Γ for each different geometry.

To illustrate the application of Eq. (12) more explicitly, we scale our measured third order intercepts shown in Fig. 3(b) to the same reference width (we choose reference values of $w_{\mathrm{ref}} = 100\,\mu\mathrm{m}$, and $\Gamma_{\mathrm{ref}} = 3\times 10^{11}\,\mathrm{m}^{-2}$):

$$P_{\mathrm{TOI}}^{\mathrm{scaled}} = P_{\mathrm{TOI}}^{\mathrm{meas}} - 20\log_{10}\left(\frac{w_s}{100}\right) + 10\log_{10}\left(\frac{\Gamma_s}{3.0\times 10^{11}}\right), \quad (14)$$

where w_s is in units of μm and Γ_s is in units of m^{-2}, and the intercept points $P_{\mathrm{TOI}}^{\mathrm{scaled}}$ and $P_{\mathrm{TOI}}^{\mathrm{meas}}$ are expressed in dBm. This scaling should effectively eliminate differences in P_{TOI} due to differences in transmission linewidth. Figure 4 shows the measured data from Fig. 3(b) scaled in this manner, which illustrates how our measured data for different linewidth devices collapse to describe roughly the same curve versus line length. This figure dramatically confirms the linewidth dependence of P_{TOI} given by Eq. (12).

We can also scale the data in Fig. 4 to take into account differences in transmission line length, also according to Eq. (12). Instead of collapsing the data a second time, we plot the length dependence predicted by Eq. (12) along with the measured data already scaled to the reference linewidth ($w_{\mathrm{ref}} = 100\,\mu\mathrm{m}$). The solid line in Fig. 4 represents such a fit to the third-order intercept versus line length using Eq. (12). The data collapse and fit illustrated in Fig. 4 demonstrate the excellent agreement between the differences in the measured

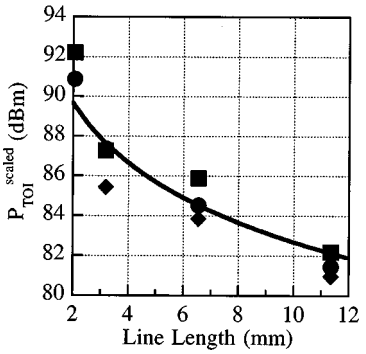

FIG. 4. Scaled third order intercepts vs line length for data shown in Fig. 3(b). The data are scaled for different linewidths to a reference geometry using Eq. (14). The solid line represents the length dependence predicted by Eq. (12). The reference geometry is given by: $w_{ref}=100\,\mu$m, $t_{ref}=500$ nm, and $\Gamma_{ref}=3\times10^{11}\,\mathrm{m}^{-2}$.

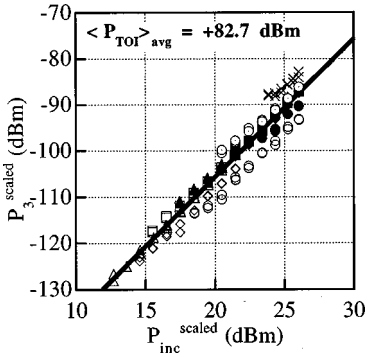

FIG. 5. Measured third harmonic vs incident power for eleven transmission lines of different geometry shown in Fig. 3(a), scaled for length and width to the same reference geometry.

P_{TOI} due to geometry and the dependence on length and width predicted by the simple model and expressed in Eq. (12).

This analysis implies that a single value for P_{TOI} can describe the twelve different geometries for the single film considered above. This value for P_{TOI} can be transformed to compare with other measurements of P_{TOI} from samples having different lengths and linewidths. In order to facilitate comparisons of different geometry samples, we adopt the convention to scale all our measured data to a fictitious reference geometry defined by a film thickness of 500 nm, a linewidth of 100 μm, and a length of 10 mm (we also use a reference value for $\Gamma=3.0\times10^{11}\,\mathrm{m}^{-2}$). We can then write the following equation to describe the scaling of P_{TOI} of any arbitrary geometry to our standard geometry:

$$P_{TOI}^{scaled}=P_{TOI}^{meas}-20\log_{10}\left[\left(\frac{w_s}{100}\right)\left(\frac{t_s}{500}\right)\right]+10\log_{10}\left[\left(\frac{L_s}{10}\right)\left(\frac{\Gamma_s}{3.0\times10^{11}}\right)\right], \quad (15)$$

with w_s expressed in μm, t_s in nm, L_s in mm, and Γ_s in m^{-2}. As before, the intercept points are expressed in dBm. A simple consequence of this analysis is that if we can scale the measured P_{TOI} for geometry, we can necessarily scale the measured third harmonic magnitude P_3 as well. The change in the magnitude of the third harmonic signal P_3 is related to the scaling correction for the third-order intercept by $\Delta P_3=-2\Delta P_{TOI}$. Figure 5 shows the third harmonic data from Fig. 3(a) scaled to the reference geometry. The resulting plot shows that the data from all lines collapse to roughly the same function, described by a line with slope 3 and a third-order intercept of $P_{TOI}=+82.7$ dBm. The ability to scale the measured P_3 data to account for geometrical differences is important for comparison of P_3 data that do not increase with incident power with slope 3 and therefore do not have a definitive third-order intercept point.

Equation (12) also predicts how our measured P_{TOI} should change for different thickness samples. Figure 6(a) shows P_{TOI} data for 21-μm-wide transmission lines fabricated from films of thickness 50, 320, and 500 nm. When scaled to the same reference thickness using Eq. (15), the variable thickness data also collapse remarkably well, as illustrated in Fig. 6(b). This application of Eq. (15) accounts for differences in the measured P_{TOI} in Fig. 6(a) of up to 25 dB. The solid line in Fig. 6(b) shows the same length dependence calculated in Fig. 4, demonstrating that samples of different thicknesses, linewidth, and line length can all be described by a single value for P_{TOI}^{scaled} using Eq. (15).

To verify that this behavior is generally valid, we perform measurements on sets of devices fabricated from a number of different films. Table I summarizes the extracted P_{TOI} scaled for geometry using Eq. (15) for several films of different thicknesses. The geometrical scaling works extremely well for all the samples considered, yielding a mean

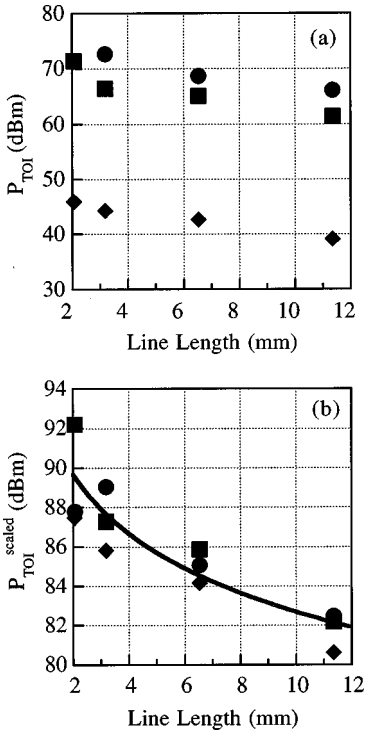

FIG. 6. (a) Measured third-order intercepts vs line length for 21 μm wide transmission lines of three different film thicknesses at 76 K: 500 nm (circles); 320 nm (squares); 50 nm (diamonds). (b) Third-order intercept data from (a) scaled for different film thicknesses using Eq. (15). The solid line is the same length dependence shown in Fig. 4.

TABLE I. Summary of third-order intercept data for several different YBCO films. Shown is the mean third-order intercept and standard deviation of the indicated number of transmission lines, after the third-order intercepts of the individual lines have been scaled to a reference geometry to account for geometrical differences. Also included is the mean nonlinear scaling current density derived from the third-order intercept and penetration depth data. The specified yield is the number of transmission lines that gave a measurable third harmonic signal of slope 3.

Film ID.	Film thickness (nm)	Yield (measurable slope 3)	Average $P_{\mathrm{TOI}}^{\mathrm{scaled}}$ (dBm)	Std. Dev. (dBm)	$J_0(10^7\ \mathrm{A/cm^2})$
L397-164	500	9/12	82.6	1.2	2.9
L397-166	500	9/12	82.1	1.1	2.8
L397-160	320	11/12	82.7	1.3	3.3
L397-161	320	10/12	82.8	1.2	3.4
L397-170	50	12/12	80.2	1.3	2.8
L397-175	50	12/12	79.5	2.5	2.6

P_{TOI} that is very similar for all samples studied. Furthermore, since we expect to obtain the same scaled P_{TOI} for all lines, we can define a standard deviation, which measures the uniformity of the scaled third order intercept across a given chip. The standard deviation in scaled third-order intercept is 1–2 dBm for all the films investigated here, which demonstrates remarkable uniformity in the nonlinear response of devices across a given chip.

This analysis is particularly simple because the only parameters we need to know accurately are the transmission line length, width, and film thickness (the geometry factor Γ is weakly dependent on the penetration depth). However, the values of P_{TOI} that we obtain are still specific to a given CPW transmission line. If, in addition, we know the penetration depth λ, we can calculate the material parameter J_0, which does not depend on geometry at all. For our samples, using values of λ measured inductively on representative samples,[18] we obtain values for J_0 in the range $2.6-3.4 \times 10^7$ A/cm^2 at 76 K, as shown in Table I. This value of J_0 is larger than the inductively measured critical current density J_c, which for these samples is measured to be $J_c \approx 3 \times 10^6$ A/cm^2. This conclusion is consistent with the results of Willemsen,[24] who find the intermodulation critical current J_{IMD} exceeds J_c for resonators fabricated from $Tl_2Ba_2CaCu_2O_{8+x}$ films.

The variation in values of $P_{\mathrm{TOI}}^{\mathrm{scaled}}$ and J_0 for different samples could be due to thickness variations in the YBCO thin film (estimated to be approximately 10% across the 15×15 mm sample) or due to temperature variations during the measurements (estimated to be approximately 1 K across the sample). The remarkable consistency in values extracted for J_0 for a large number of transmission lines of different geometries demonstrates that the nonlinear scaling current density for these samples can be considered to be an intrinsic material property.

V. CONCLUSIONS

A simple model based on a current-dependent penetration depth accurately describes measurements of third harmonic generation in CPW transmission lines fabricated from YBCO thin films. This model quantitatively explains the measured differences in harmonic generation for different CPW dimensions, including film thickness, center conductor linewidth and line length, suggesting that the observed nonlinearities are an intrinsic material property. This analysis is used along with a simple measurement system to demonstrate the removal of geometrical effects from measurements of the nonlinear response in HTS devices. Our results can be used along with the theory of Dahm and Scalapino[14] to predict the limits on nonlinearity for practical superconducting devices of arbitrary geometries at microwave frequencies. The nonlinear scaling current density J_0 obtained from these measurements at 76 K is remarkably consistent for all the samples studied and also provides an appropriate figure of merit for optimizing fabrication processes to minimize material-dependent nonlinear effects. We plan to use these methods in future work to determine the relative importance of pattering techniques and film growth conditions on nonlinearities in the HTS materials. In addition, we plan to investigate the temperature dependence of the observed nonlinear effects (through the temperature dependence of $P_{\mathrm{TOI}}^{\mathrm{scaled}}$ and J_0) in a manner analagous to Ref. 24 in order to further understand their physical origin.

ACKNOWLEDGMENTS

The authors gratefully acknowledge Balam Willemsen of Superconductor Technologies, Inc., and Thomas Dahm of the Max Planck Institute for Physics of Complex Systems for extremely helpful discussions regarding the calculation of harmonic products from a nonlinear inductance. We also thank Don DeGroot of NIST and Chris Holloway of the Institute for Telecommunication Sciences for helpful comments on the manuscript. We also acknowledge John Claassen at the Naval Research Labs for performing the penetration depth measurements, and the Office of Naval Research for funding support. The contribution of J.C.B. was supported in part by a NIST/National Research Council Postdoctoral Associateship.

[1] Z. Y. Shen, *High-Temperature Superconducting Microwave Circuits* (Artech House, Boston, 1994).
[2] G.-C. Liang, D. Zhang, C.-F. Shih, M. E. Johansson, R. S. Withers, D. E. Oates, A. C. Anderson, P. Polakos, P. Mankiewich, E. de Obaldia, and R. E. Miller, IEEE Trans. Microwave Theory Tech. **43**, 3020 (1995).
[3] D. E. Oates, A. C. Anderson, D. M. Sheen, and S. M. Ali, IEEE Trans. Microwave Theory Tech. **39**, 1522 (1991).
[4] P. P. Nguyen, D. E. Oates, G. Dresselhaus, and M. S. Dresselhaus, Phys. Rev. B **48**, 6400 (1993).
[5] C. Wilker, Z.-Y. Shen, P. Pang, W. L. Holstein, and D. W. Face, IEEE Trans. Appl. Supercond. **5**, 1665 (1995).
[6] For examples and descriptions of the different planar geometries, see, K. C. Gupta, R. Garg, I. Bahl, and P. Bhartia, *Microstrip Lines and Slotlines*, 2nd ed. (Artech House, Boston, 1996).
[7] Z. Ma, E. de Obaldia, G. Hampel, P. Polakos, P. Mankiewich, B. Batlogg, W. Prusseit, H. Kinder, A. Anderson, D. E. Oates, R. Ono, and J. Beall, IEEE Trans. Appl. Supercond. **7**, 1911 (1997).
[8] B. A. Willemsen, T. Dahm, and D. J. Scalapino, Appl. Phys. Lett. **71**, 3898 (1997).
[9] Y. Yoshitake, S. Tahara, and S. Suzuki, Appl. Phys. Lett. **67**, 3963 (1995).
[10] J. P. Hong and J. S. Lee, Appl. Phys. Lett. **68**, 3034 (1996).
[11] G. Hampel, B. Batlogg, K. Krishana, N. P. Ong, W. Prusseit, H. Kinder, and A. C. Anderson, Appl. Phys. Lett. **71**, 3904 (1997).
[12] S. A. Mass, *Nonlinear Microwave Circuits* (Artech House, Boston, 1988).

[13] J. C. Booth, J. A. Beall, R. H. Ono, F. J. B. Stork, D. A. Rudman, and L. R. Vale, Appl. Supercond. **5**, 379 (1998).
[14] T. Dahm and D. J. Scalapino, J. Appl. Phys. **81**, 2002 (1997).
[15] D. E. Oates, Y. M. Habib, C. J. Lehner, L. R. Vale, R. H. Ono, G. Dresselhaus, and M. S. Dresselhaus, IEEE Trans. Appl. Supercond. (to be published).
[16] J. McDonald, J. R. Clem, and D. E. Oates, Phys. Rev. B **55**, 11823 (1997).
[17] The quoted temperature is that of the heater block. The actual substrate temperature during deposition may be 50–70 °C less.
[18] J. H. Claassen, M. L. Wilson, J. M. Byers, and S. Adrian, J. Appl. Phys. **82**, 3028 (1997).
[19] J. C. Booth, J. A. Beall, D. C. DeGroot, D. A. Rudman, R. H. Ono, J. R. Miller, M. L. Chen, S. H. Hong, and Q. Y. Ma, IEEE Trans. Appl. Supercond. **7**, 2780 (1997).
[20] To see the relation of P_{TOI} to the more commonly specified y intercept, consider the third harmonic data to be described by a line of intercept b and slope 3: $\log P_3 = b + 3 \log P_{\mathrm{inc}}$. The fundamental is described by a line of slope 1 with zero intercept: $\log P_1 = 1 \log P_{\mathrm{inc}}$. The third order intercept is determined by the value of P_{inc} at which $\log P_3 = \log P_1$. This gives $\log P_{\mathrm{TOI}} = -b/2$.
[21] R. B. Hammond, E. R. Soars, B. A. Willemsen, T. Dahm, D. J. Scalapino, and J. R. Schrieffer, J. Appl. Phys. **84**, 5662 (1998).
[22] J. C. Booth, J. A. Beall, L. R. Vale, and R. H. Ono, 53rd ARFTG Digest (in press).
[23] D. M. Sheen, S. M. Ali, D. E. Oates, R. S. Withers, and J. A. Kong, IEEE Trans. Appl. Supercond. **1**, 108 (1991).
[24] B. A. Willemsen, K. E. Kihlstrom, T. Dahm, D. J. Scalapino, B. Gowe, D. A. Bonn, and W. N. Hardy, Phys. Rev. B **58**, 6650 (1998).